scientific reports

Check for updates

OPEN

Preparation and improvement electrochemical performance of Ni-Fe doped porous $LiMnPO_4$/C materials

Jilan Li[1,2]✉, Zhangbin Liu[2] & Jiarou Ma[2]

Lithium manganese phosphate ($LiMnPO_4$) is the most promising candidate for the next generation of lithium-ion battery cathode materials due to its 4.1 V(vs. Li/Li^+) high voltage platform. At present, the discharge rate performance and cycle stability are still poor. And here, various Fe, Ni co-doped carbon-coated $LiMnPO_4$ composites materials $LiMnPO_4$/C were successfully prepared using coprecipitation and solvothermal methods. Morphological and electrochemical performance analyses were conducted on the $LiMnPO_4$/C materials prepared by different methods to explore the relationship between material morphology and electrochemical performance. Compared with the coprecipitation method, $LiMnPO_4$/C prepared by the solvothermal method has a smaller particle size and a more regular morphology. Moreover, after the addition of glucose as an auxiliary, the particles exhibit a spindle-shaped porous structure, leading to improved cycling performance and rate capability, and demonstrating superior electrochemical properties. At 0.1, 0.2, 0.5, 1, and 2 C, the discharge specific capacities are 121.4, 102.7, 91.2, 81.5, and 53.7 mAh g^{-1}, respectively. After 100 cycles at 1 C rate, 91% of the initial capacity is still retained. The above results indicate selecting appropriate preparation methods and controlling the structure and morphology of the material, the electrochemical activity of $LiMnPO_4$ can be directly influenced, which providing a new approach to improve the electrochemical performance of $LiMnPO_4$.

Keywords Lithium-ion battery, Cathode material, $LiMnPO_4$, Fe-Ni co-doped, Solvothermal method

With the depletion of fossil resources and the increasing demand for energy, energy crises and environmental pollution have become two major global challenges[1,2]. Low-carbon, green, and efficient renewable energy has become a key focus of research and development[3–6]. Lithium-ion batteries (LIBs) are currently widely used in portable electronic devices, electric vehicles, and large-scale energy storage systems due to their high energy density, long cycle life, and environmentally friendly nature[7–10]. As a crucial component of LIBs, the cathode material determines the performance and price of LIBs[11–13]. Among them, olivine-type lithium transition metal phosphates ($LiMPO_4$, M = Mn, Fe, Co, Ni) have been widely studied and applied as LIBs cathode materials in recent years[14–21]. This is due to the strong P-O covalent bonds and stable three-dimensional framework structure of PO_4^{3-}, which prevents structural rearrangement during Li^+ insertion/extraction, resulting in good structural stability.

Since its first synthesis and report by Goodenough's research group in 1997, $LiFePO_4$ has been widely used as a cathode material in lithium-ion batteries due to its advantages of good stability, environmental friendliness, and low cost[22–24]. Despite these advantages, lithium iron phosphate (LFP) is limited by its low theoretical capacity(170 mAh g^{-1}), in particular, the Fe^{2+}/Fe^{3+} redox couple results in a relatively low discharge voltage plateau (3.4 V vs. Li/Li^+) for $LiFePO_4$, leading to a low theoretical energy density (578 Wh kg^{-1}) and severely hindering its application in power batteries[25–28]. In contrast, $LiMnPO_4$ also possesses an olivine structure and exhibits a higher voltage plateau of 4.1 V (vs. Li/Li^+), a theoretical capacity similar to $LiFePO_4$ (170 mAh g^{-1}), and an energy density approximately 20% higher than $LiFePO_4$. It also has advantages such as low toxicity, safety, and low cost, making it better suited to meet the high energy density requirements of next-generation lithium-ion batteries[29–31]. Notably, the operating potential of $LiMnPO_4$ is compatible with the voltage window of most currently used lithium-ion battery electrolytes, making it an ideal alternative to $LiFePO_4$ as a cathode

[1]School of Chemistry and Materials Engineering, Liupanshui Normal University, Liupanshui, Guizhou 553004, China. [2]College of Environmental and Chemical Engineering, Dalian University, Dalian, Liaoning 116622, China. ✉email: lihaiqing998@163.com

material[32,33]. However, the extremely low electronic conductivity and Li^+ migration rate of $LiMnPO_4$ lead to poor rate performance, posing the biggest challenge to its development[11]. Furthermore, the Jahn-Teller effect of Mn^{3+} in the delithiated phase $MnPO_4$ causes lattice distortion and excessive volume change during Li^+ insertion/extraction, resulting in poor cycle stability of $LiMnPO_4$ batteries. These factors hinder the commercial application of $LiMnPO_4$ batteries and represent significant challenges for the development of $LiMnPO_4$ cathode materials[29,34].

Currently, strategies such as carbon coating, ion doping, and material nanostructuring are primarily employed to enhance the electrochemical performance of $LiMnPO_4$[35–37]. Among these, cation doping has become a common method for improving the electrochemical properties of $LiMnPO_4$. For example, Khalfaouy et al.[38]. prepared Ni-doped $LiMnPO_4$ material, $LiMn_{1-x}Ni_xPO_4$ (x = 0.00-0.05), and found that nickel doping significantly improved the cycle stability and rate performance of $LiMnPO_4$. Li et al.[39]. synthesized Fe-doped $LiMn_{0.8}Fe_{0.2}PO_4$/C composite material via a solid-state method using different iron sources. The results showed that iron doping could also significantly improve the rate performance and cycle performance of $LiMnPO_4$. Simultaneously, optimizing the morphology to improve the transport properties of $LiMnPO_4$ has also become a research focus. Morphology and particle size control are crucial for Li^+ diffusion in $LiMnPO_4$ and significantly affect its rate performance, representing an effective pathway to achieve high-performance of $LiMnPO_4$[21,40–42]. Among various preparation methods, the solvothermal method not only promotes a complete reaction of reactants but also allows for simpler control of crystal morphology by adjusting the supersaturation of the solution through temperature and pressure control. This method is widely used for the synthesis of $LiMnPO_4$ materials with various morphologies[43–45].

Currently, most studies employ single-element doping methods to improve the electrochemical performance of $LiMnPO_4$, while research on double-element doping is relatively limited. Based on previous studies of nickel and iron doping, this work adopts a Fe, Ni double-doping strategy (molar ratio of Mn: Fe: Ni = 0.85:0.075:0.075) to synthesize three carbon-coated $LiMnPO_4$/C composites using co-precipitation and solvothermal methods, respectively. The prepared $LiMnPO_4$/C composites are then characterized by X-ray diffraction (XRD), scanning electron microscopy (SEM), and galvanostatic charge-discharge tests. The influence of different synthesis methods on the morphology and electrochemical performance of Fe, Ni double-doped $LiMnPO_4$/C was comparatively studied.

Materials and methods

Preparation of $LiMnPO_4$ and $LiMnPO_4$/C composites

Three Ni, Fe co-doped $LiMnPO_4$/C composite materials were prepared using co-precipitation and solvothermal methods, respectively. The molar ratio of Mn: Fe: Ni is 0.85:0.075:0.075 in all cases. All reagents used in this work are analytical reagent (AR) grade. These include lithium hydroxide ($LiOH{\cdot}H_2O$, Tianjin Kemiou Chemical Reagent Co., Ltd.), phosphoric acid (H_3PO_4, Xilong Science), manganese sulfate ($MnSO_4{\cdot}H_2O$, Xilong Science), ferrous sulfate ($FeSO_4{\cdot}7H_2O$, Xilong Science), ethylene glycol ($C_2H_6O_2$, Xilong Science), nickel nitrate ($Ni(NO_3)_2{\cdot}6H_2O$, Shanghai Reagent Second Factory), glucose ($C_6H_{12}O_6$, Sinopharm Chemical Reagent Co., Ltd.), sucrose ($C_{12}H_{22}O_{11}$, Chengdu Jinshan Chemical Reagent Co., Ltd.), and cetyltrimethylammonium bromide (CTAB) ($(C_{16}H_{33})N(CH_3)_3Br$, Sinopharm Chemical Reagent Co., Ltd.).

Co-precipitation method: First, 0.0425 mol $MnSO_4{\cdot}H_2O$ was dissolved in 30 ml deionized water, and 0.0425 mol H_3PO_4 was dissolved in 10 ml deionized water separately. The H_3PO_4 solution was added to the $MnSO_4{\cdot}H_2O$ solution and stirred for 1 h. Then 0.1275 mol $LiOH{\cdot}H_2O$ and 0.075 g CTAB (0.1 wt%) were added to the above mixture under continuous stirring until a brown uniform solution is obtained, labelled solution A1. Second, 0.00375 mol $FeSO_4{\cdot}7H_2O$ and 0.00375 mol $Ni(NO_3)_2{\cdot}6H_2O$ were dissolved in 15 ml deionized water under stirring, 0.0075 mol H_3PO_4 was dissolved in 5 ml deionized water additionally, and this H_3PO_4 solution was added dropwise to the mixed $FeSO_4{\cdot}$ and $Ni(NO_3)_2$ solution and stirred at room temperature for 1 h. Then 0.0225 mol $LiOH{\cdot}H_2O$ and 0.035 g CTAB were slowly added dropwise to the above solution and continue stirred at room temperature for 1 h, labelled solution A2. Third, solution A1 and solution A2 were mixed and stirred magnetically at 50 ℃ for 6 h. After standing overnight, the precipitate was separated by centrifugation. The precipitate was dried at 80 ℃ for 12 h in a drying oven to obtain a precursor. The precursor was mixed with a sucrose aqueous solution(precursor to sucrose mass ratio of 2:1) and stirred for 2 h. The mixture was then dried at 80 ℃ for 24 h in a drying oven. Finally, the mixture was sintered at 600 ℃ for 5 h under N_2 atmosphere to obtain $LiMnPO_4$/C, denoted as $LiMnPO_4$/C-A.

Solvothermal method: Based on the co-precipitation method described above, the difference is that the solvent is replaced with a mixture of glycol and water (volume ratio 1:1), the resulting B1 and B2 mixed solution was transferred to a hydrothermal autoclave and maintained at 180 ℃ for 10 h. After centrifugation and drying, the precursor was mixed with sucrose (precursor to sucrose mass ratio of 2:1) in an aqueous solution and stirred for 2 h as the precipitation method mentioned above. Then drying and calcination and mixing with sucrose like the precipitation method mentioned above and the resulting material was labeled $LiMnPO_4$/C-B. Additionally, $LiMnPO_4$/C was prepared using the same solvothermal method, the difference is that 1 gram of glucose was added during the hydrothermal process, and the resulting material was labeled $LiMnPO_4$/C-C. The preparation process of $LiMnPO_4$/C-C is illustrated in Fig. 1.

Material characterization

The phase structures of all synthesized samples were analyzed by X-ray diffraction (XRD, Shimadzu XRD-6100) using Cu Kα radiation in the 2θ range of 5–80°. The morphologies of the synthesized samples were characterized using field emission scanning electron microscopy (FE-SEM, Hitachi SU8010). The elemental distribution of the $LiMnPO_4$/C-C sample was analyzed by energy-dispersive X-ray spectroscopy (EDS, Horiba EMAX). The

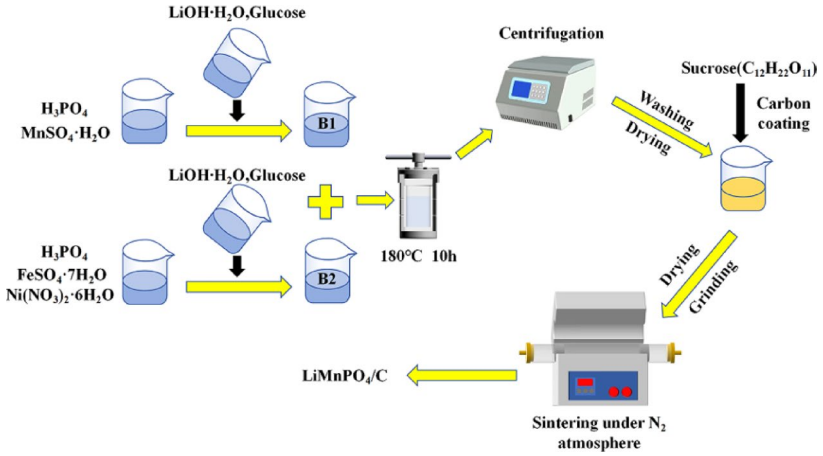

Fig. 1. Schematic preparation process of $LiMnPO_4$/C-C cathode materials.

specific surface area and pore size distribution of the samples were characterized by nitrogen adsorption/desorption isotherms at 77 K obtained using a surface area and porosity analyzer (Micromeritics ASAP2460).

Electrochemical tests

The active material, acetylene black, and polyvinylidene fluoride (PVDF) were mixed in a weight ratio of 80:10:10, respectively (the active material loading is 1.5 mg). The mixture was homogenized by stirring in N-methyl-2-pyrrolidone (NMP) for 6 h to form a slurry. This slurry was then uniformly coated onto an aluminum foil current collector using a coating machine (Shenzhen Kejing MSK-AFAE-S200). The resulting electrode was dried overnight at 80 °C. The electrode was transferred to an argon-filled glove box (Vigor SG1200/750TS) and used as the positive electrode in a CR2025 coin cell. A Celgard 2400 membrane served as the separator, lithium foil as the negative electrode, and 1 M $LiPF_6$ solution in ethylene carbonate (EC): diethyl carbonate (DEC): dimethyl carbonate (DMC) (volume ratio 1:1:1) as the electrolyte.

Constant current charge-discharge tests were performed using a Land CT3002A battery tester within a voltage range of 2.5–4.5 V. Electrochemical impedance spectroscopy (EIS) measurements were conducted on a Princeton Applied Research VersaSTAT 3 electrochemical workstation over a frequency range of 10^{-2} to 10^5 Hz. All tests were performed at 25 °C.

Results and discussion

XRD and SEM analysis

Figure 2 shows the XRD patterns of the three prepared samples: $LiMnPO_4$/C-A, $LiMnPO_4$/C-B, and $LiMnPO_4$/C-C. All three samples show good agreement with the $LiMnPO_4$ standard PDF# 33–0803, this indicates that $LiMnPO_4$/C were prepared successsfully. The absence of carbon diffraction peaks may be attributed to the amorphous nature of the carbon[36]. On the other hand, the lack of iron and nickel peaks may be due to their low concentrations being masked by the manganese signal, there is a number marked as nickel peak. All XRD peaks match those of $LiMnPO_4$, with no additional peaks present, indicating that nickel-iron doping has been incorporated into the $LiMnPO_4$ crystal lattice.

The morphologies of the three samples, $LiMnPO_4$/C-A, $LiMnPO_4$/C-B, and $LiMnPO_4$/C-C, are shown in Fig. 3. The co-precipitation method produced $LiMnPO_4$/C-A with an irregular morphology and large particle size, exhibiting non-nanoscale agglomeration. The solvothermal method yielded $LiMnPO_4$/C-B with a more regular rod-like morphology, approximately 100 nm in width and 200–300 nm in length. The glucose-assisted solvothermal method produced $LiMnPO_4$/C-C with a regular, spindle-shaped, porous structure. The particle size of $LiMnPO_4$/C-C is similar to $LiMnPO_4$/C-B, but with a more uniform distribution. Further TEM characterization revealed the porous structure of $LiMnPO_4$/C-C, Fig. 5 clearly shows the distinct porous structure of $LiMnPO_4$/C-C, in contrast to $LiMnPO_4$/C-A and $LiMnPO_4$/C-B which lack porosity. The uniformly small particles are beneficial for shortening the Li^+ diffusion pathways, while the porous structure facilitates increased contact with the electrolyte[33,46].

To further determine the elemental composition and distribution of the $LiMnPO_4$/C-C nanomaterial, energy dispersive spectroscopy (EDS) and elemental mapping were performed on the prepared $LiMnPO_4$/C-C material, with the results shown in Fig. 4. Figure 4 shows that Fe, Ni, and C elements are uniformly distributed throughout the $LiMnPO_4$/C-C sample, indicating successful doping of Fe and Ni into the $LiMnPO_4$ material.

To further characterize the porous structure of the synthesized $LiMnPO_4$/C-C, nitrogen adsorption-desorption tests were performed on the prepared $LiMnPO_4$/C-C, and the results are shown in Fig. 6. The BET surface area of $LiMnPO_4$/C-C is 63.0 m^2g^{-1}, and the pore volume is 0.12 cm^3g^{-1}. The adsorption-desorption isotherm (Fig. 6a) is a typical type IV isotherm, exhibiting a clear hysteresis loop at higher nitrogen pressure, indicating a mesoporous structure of $LiMnPO_4$/C-C[47]. Figure 6b shows that the $LiMnPO_4$/C-C has an unimodal pore-size distribution with a average pore diameter of 7.46 nm. The large surface area provides more active sites for Li^+ insertion/extraction, and the nanoporous structure contributes to an improved Li^+ diffusion rate.

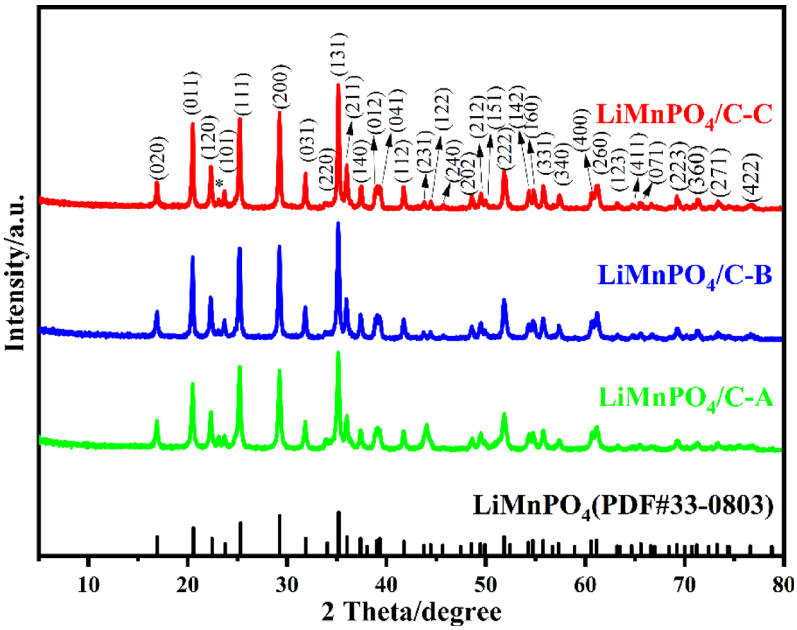

Fig. 2. XRD patterns of $LiMnPO_4$/C-A, LiMnPO4/C-B and $LiMnPO_4$/C-C.

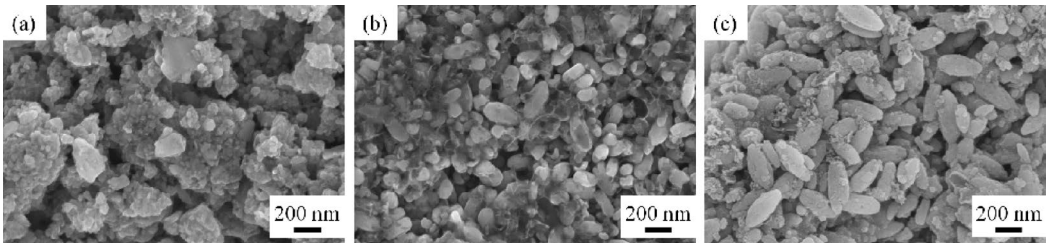

Fig. 3. SEM images of (**a**) $LiMnPO_4$/C-A, (**b**) $LiMnPO_4$/C-B and (**c**) $LiMnPO_4$/C-C.

Figure 7 presents the XPS analysis of $LiMnPO_4$/C-A, $LiMnPO_4$/C-B, and $LiMnPO_4$/C-C. The survey scan reveals the presence of nickel (Ni) and iron (Fe) elements. Furthermore, the Mn 2p peak is consistent with that reported in the literature for Fe-doped $LiMnPO_4$, while the Fe2p peak ($Fe2p_{3/2}$:710.73, 711.05, 709.56 eV, $Fe2p_{1/2}$:723.76, 724.34, 724.16 eV), matches that reported for $LiMn_{0.9}Fe_{0.1}PO_4$[48]. Based on the preceding XRD and elemental mapping analyses, it can be concluded that nickel- and iron-doped $LiMnPO_4$ has been successfully synthesized.

Electrochemical performance of $LiMnPO_4$/C composites

Figures 8 and 9 show the charge-discharge curves and rate performance of $LiMnPO_4$/C-A, $LiMnPO_4$/C-B, and $LiMnPO_4$/C-C, respectively. Figure 8 reveals that all three materials exhibit a discharge plateau around 4.1 V, consistent with most literature reports on $LiMnPO_4$, further confirming the successful synthesis of $LiMnPO_4$. At 0.1 C, the co-precipitation method prepared $LiMnPO_4$/C-A shows a maximum discharge capacity of 45.9 mAh g^{-1}, the solvothermal method prepared $LiMnPO_4$/C-B exhibits a maximum discharge capacity of 117.9 mAh g^{-1}, and the glucose-assisted solvothermal method prepared $LiMnPO_4$/C-C shows a maximum discharge capacity of 121.4 mAh g^{-1}. Clearly, the solvothermal methods significantly improve the maximum discharge capacity of $LiMnPO_4$/C. Figure 9 shows that the discharge capacities of $LiMnPO_4$/C-A, $LiMnPO_4$/C-B, and $LiMnPO_4$/C-C are 2 mAh g^{-1}, 4.7 mAh g^{-1}, and 53.7 mAh g^{-1} at 2 C, respectively. $LiMnPO_4$/C-C demonstrates superior rate performance, indicating that glucose significantly enhances the rate capability of the $LiMnPO_4$/C material.

Figure 10 presents the discharge cycling performance of $LiMnPO_4$/C-B and $LiMnPO_4$/C-C at 1 C for 100 cycles. $LiMnPO_4$/C-B exhibits a capacity retention of 80.7%, while $LiMnPO_4$/C-C shows a significantly improved capacity retention of 91.0%. This indicates that the $LiMnPO_4$/C-C material, with its regular, nanostructured, spindle-like morphology, possesses superior cycling stability. Combining this with the previous morphological and structural analysis, it is found that the $LiMnPO_4$/C-C material, with its regular, nanostructured, spindle-like porous structure, not only shows significant improvements in discharge capacity and rate performance but also exhibits greatly enhanced discharge cycling stability. Table 1 compares the electrochemical performance of this material with that of $LiMnPO_4$ materials reported in recent literature.

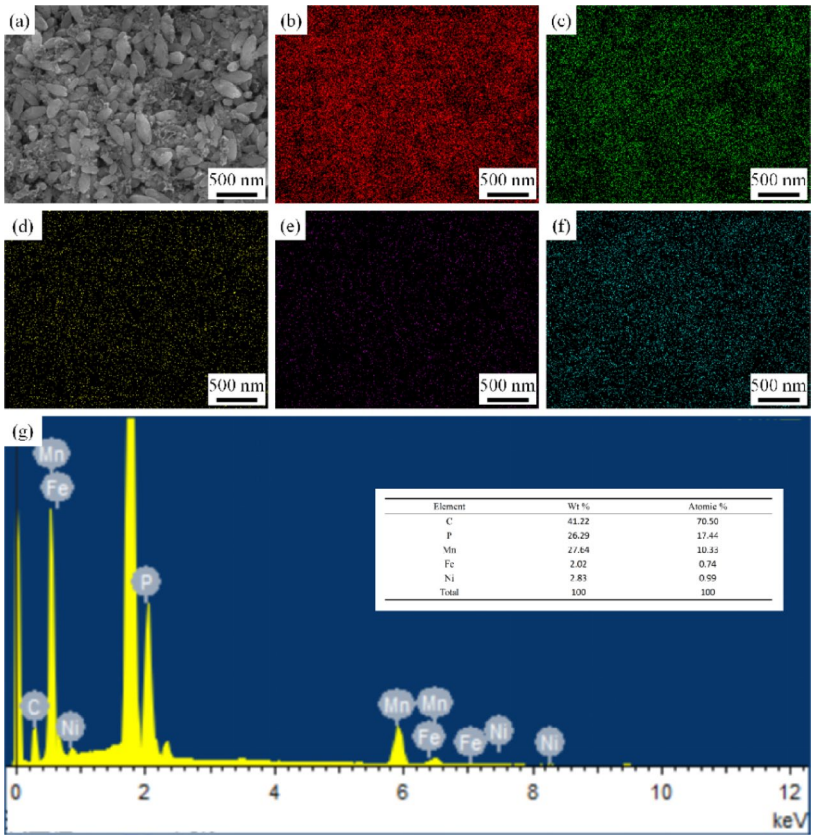

Fig. 4. SEM images of $LiMnPO_4$/C-C (**a**), EDS elemental mappings of P、Mn、Fe、Ni and C in $LiMnPO_4$/C-C respectively (**b**-**f**) and proportion of elements(**g**).

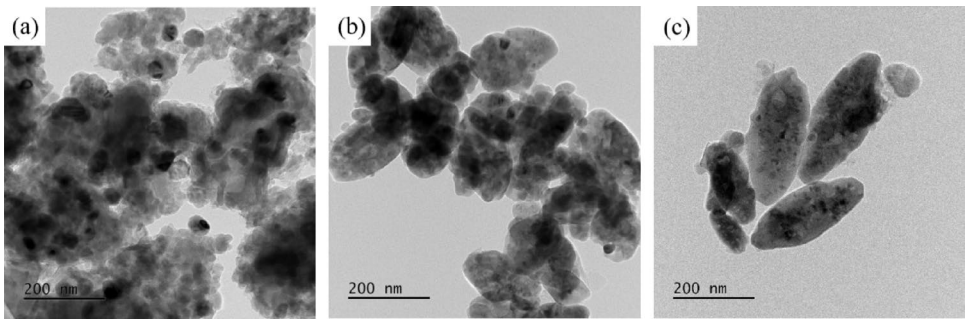

Fig. 5. TEM images of (**a**) $LiMnPO_4$/C-A, (**b**) $LiMnPO_4$/C-B and (**c**) $LiMnPO_4$/C-C.

Figure 11 shows the Nyquist plots and equivalent circuit diagrams for $LiMnPO_4$/C-A, $LiMnPO_4$/C-B, and $LiMnPO_4$/C-C electrodes. The inset table presents the fitting data of the EIS curves. The curves consist of a semicircle in the high-frequency region and a sloping line in the low-frequency region. The diameter of the semicircle corresponds to the charge transfer resistance (Rct) between the electrode and the electrolyte, while the intercept of the semicircle on the Z' axis is attributed to the solution resistance (Rs). The slope of the inclined line (Zw) represents the Warburg impedance, corresponding to the diffusion of Li^+ ions in the bulk material[22,34,53]. The Rct values for $LiMnPO_4$/C-A, $LiMnPO_4$/C-B, and $LiMnPO_4$/C-C electrodes are 204.1, 76.8, and 64.9 Ω, respectively, indicating that $LiMnPO_4$/C-C exhibits a faster electrochemical response and better kinetic performance. Furthermore, the slope of the inclined line in the low-frequency region is steeper for the $LiMnPO_4$/C-C electrode than for $LiMnPO_4$/C-A and $LiMnPO_4$/C-B, indicating a smaller Zw and a faster Li^+ diffusion rate. The EIS results demonstrate that $LiMnPO_4$/C-C possesses superior electrochemical kinetics, further validating the interpretations of the previous charge-discharge and cycling performance test results.

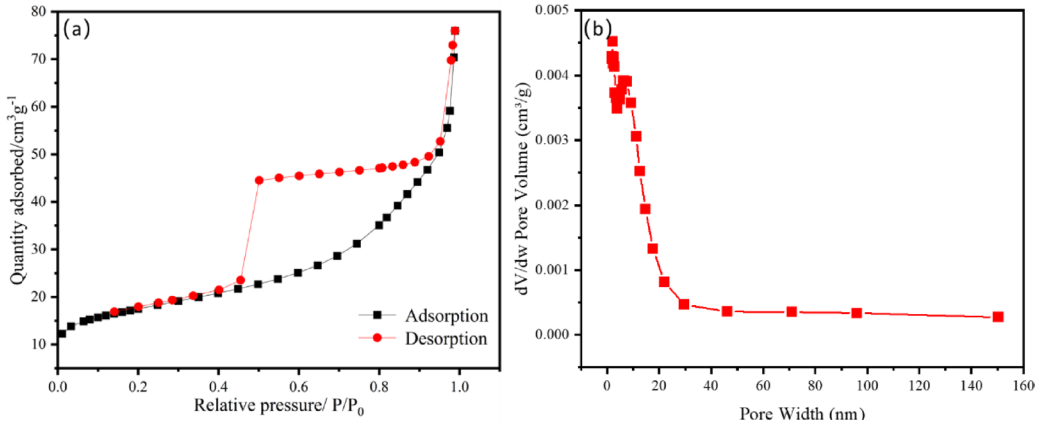

Fig. 6. Nitrogen adsorption-desorption isotherm(**a**) and pore size distribution curves(**b**) of $LiMnPO_4$/C-C.

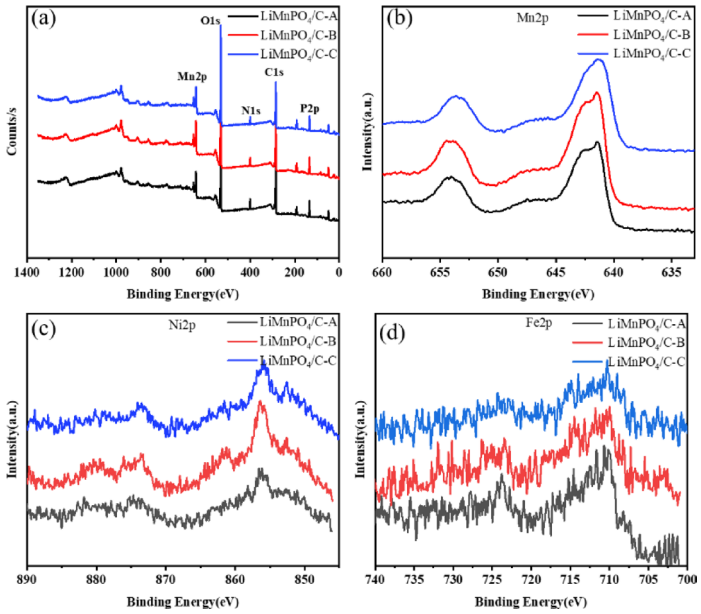

Fig. 7. XPS spectrum overall spectrum (**a**), Mn2p (**b**), Ni2p (**c**) and Fe2p (**d**) for $LiMnPO_4$/C-A, $LiMnPO_4$/C-B and $LiMnPO_4$/C-C.

Conclusions

A variety of Fe and Ni doping $LiMnPO_4$ composites were prepared through three different methods : $LiMnPO_4$/C-A, $LiMnPO_4$/C-B, and $LiMnPO_4$/C-C. Comparative analysis reveals that the $LiMnPO_4$/C-C material prepared by a glucose-assisted solvothermal method exhibits smaller particle size and a more regular morphology compared to the co-precipitation method, and the material displays a spindle-shaped porous structure. Benefiting from this nanosize, regular morphology and porous structure, the battery prepared using this material shows significantly improved rate performance and cycling performance, demonstrating superior electrochemical properties. Their discharge capacities are achieved of 121.4, 102.7, 91.2, 81.5, and 53.7 mAh g^{-1} at 0.1, 0.2, 0.5, 1, and 2 C rates, respectively, and the capacity retention reaches 91% after 100 charge-discharge cycles at 1 C. This demonstrates that selecting an appropriate preparation method and controlling the morphology and structure of the material are crucial for optimizing the electrochemical performance of $LiMnPO_4$. This study provides a basis and guidance for further optimization of the electrochemical performance of $LiMnPO_4$ materials.

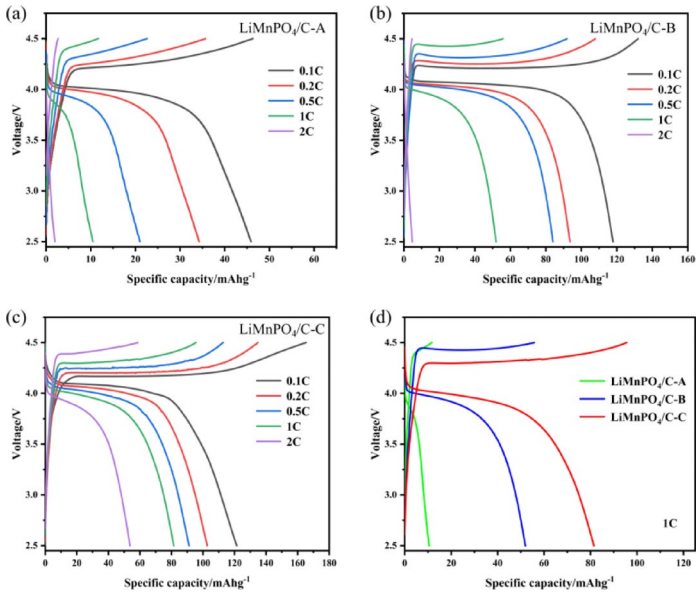

Fig. 8. Charge-discharge curves (**a**-**c**) and specific capacity comparison (**d**) of $LiMnPO_4$/C-A, $LiMnPO_4$/C-B and $LiMnPO_4$/C-C samples at 1 C.

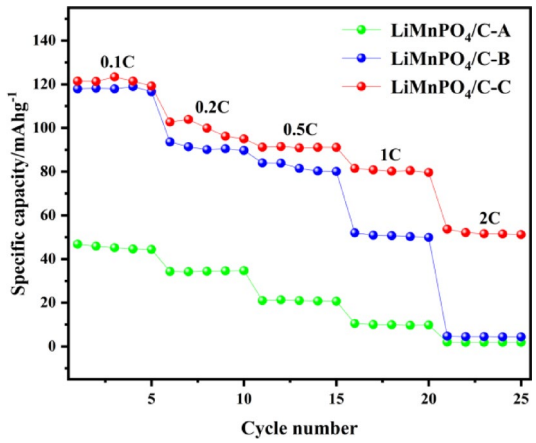

Fig. 9. Discharge capacity of $LiMnPO_4$/C-A, $LiMnPO_4$/C-B and $LiMnPO_4$/C-C samples at different rates.

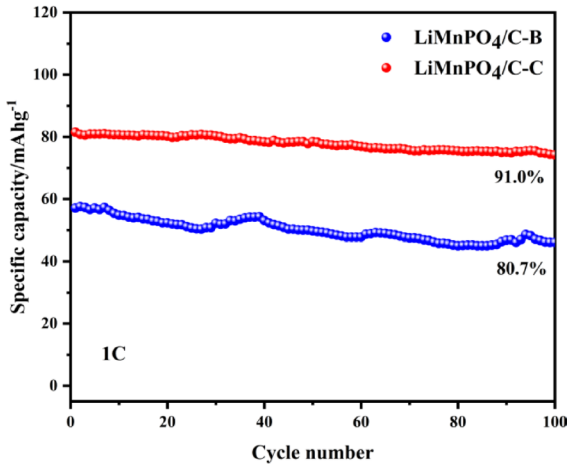

Fig. 10. Cycle performance of $LiMnPO_4$/C-B and $LiMnPO_4$/C-C.

Cathode material	Actual capacity(mAh g^{-1})	Cycling performance	Refs.
$LiMnPO_4$-SS	89.15(at 0.2 C)	99%(50 cycles)	[49]
$LiMnPO_4$	84(at 0.2 C)	—	[50]
$LiMnPO_4$	89.8(at 0.05 C)	80%(30 cycles)	[16]
$LMnPO_4$/C	80.2(at 0.1 C)	—	[51]
$LiMnPO_4$	91.5(at 0.2 C)	25%(50 cycles)	[52]
$LiMnPO_4$/C	102.7(at 0.2 C)	91%(100 cycles)	this work

Table 1. Comparison of electrochemical performance for different $LiMnPO_4$ materials.

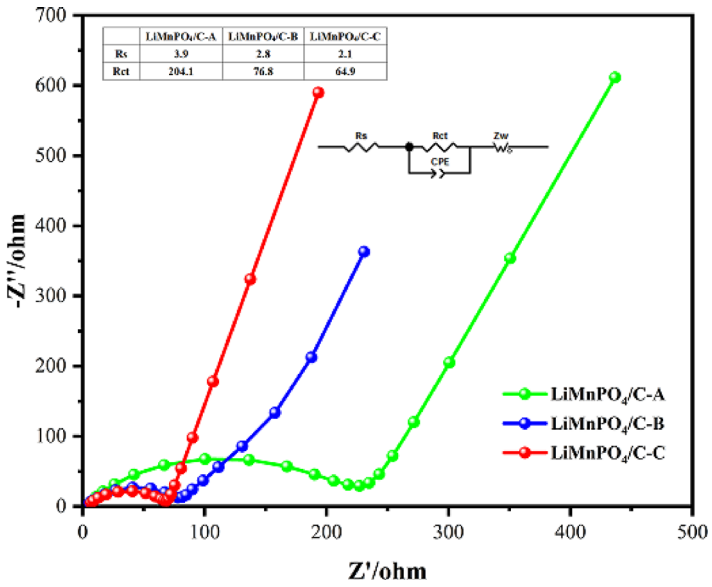

Fig. 11. EIS of $LiMnPO_4$/C-A, $LiMnPO_4$/C-B and $LiMnPO_4$/C-C.

Data availability

The authors declare that the data supporting the findings of this study are available within the paper, and the data that support the findings of this study are available from the corresponding author upon reasonable request.

Received: 31 March 2025; Accepted: 21 July 2025
Published online: 31 July 2025

References

1. Wu, F., Maier, J. & Yu, Y. Guidelines and trends for next-generation rechargeable lithium and lithium-ion batteries. *Chem. Soc. Rev.* **49** (5), 1569–1614 (2020).
2. Iqbal, M. Z., Abbasi, U. & Alzaid, M. Cobalt manganese phosphate and sulfide electrode materials for potential applications of battery-supercapacitor hybrid devices. *J Energy Storage*, **50** 104632.1-104632.11.(2022)
3. Xue, Z. et al. Sodium doping to enhance electrochemical performance of overlithiated oxide cathode materials for Li-Ion batteries via li/na Ion-exchange method. *ACS Appl. Interfaces*. **10** (32), 27141–27149 (2018).
4. Wu, L. et al. PPy-encapsulated SnS_2 nanosheets stabilized by defects on a TiO_2 support as a durable anode material for Lithium-Ion Batteries. *Angew Chem. Int. Ed.* **58** (3), 811–815 (2018).
5. Chen, W. et al. Mn-doped $LiFePO_4$@C as a high-performance cathode material for lithium-ion batteries. *Particuology* **90**, 418–428 (2024).
6. Wang, G. et al. Chemically activated Hollow carbon nanospheres as a high-performance anode material for potassium ion batteries. *J. Mater. Chem. A*. **6** (47), 24317–24323 (2018).
7. Zhang, T. W. et al. Recent advances on biopolymer fiber based membranes for lithium-ion battery separators. *Compos. Commun.* **14**, 7–14 (2019).
8. Ragupathi, V., Panigrahi, P. & Nagarajan, G. S. Enhanced electrochemical performance of nanopyramid-like $LiMnPO_4$/C cathode for lithium-ion batteries. *Appl Surf. Sci*, **495**(30): (2019). 143541.1-143541.6.
9. Pender, J. P. et al. Electrode degradation in lithium-Ion batteries. *ACS Nano*. **14** (2), 1243–1295 (2020).
10. Gu, K. et al. Efficient separation of cathode materials and al foils from spent lithium batteries with glycerol heating: A green and unconventional way[J]. *J Clean. Prod*, **369**(1)133270.1-133270.9.(2022)
11. Yang, L. et al. Olivine $LiMn_xFe_{1-x}PO_4$ cathode materials for lithium ion batteries: restricted factors of rate performances. *J. Mater. Chem. A*. **9** (25), 14214–14232 (2021).
12. Yang, J. et al. Green synthesis of high-performance $LiFePO_4$ nanocrystals in pure water. *Green. Chem.* **20** (22), 5215–5223 (2018).
13. Deng, Z. et al. Fast precipitation-induced $LiFe_{0.5}Mn_{0.5}PO_4$/C nanorods with a fine size and large exposure of the (010) faces for high-performance lithium-ion batteries. *J. Alloy Compd.* **794**, 178–185 (2019).
14. Zou, B. et al. Solvothermal synthesized $LiMn_{1-x}Fe_xPO_4$@C nanopowders with excellent high rate and low temperature performances for lithium-ion batteries. *RSC Adv.* **6** (57), 52271–52278 (2016).
15. Chen, W. et al. Rational design of nano-structured ammonium manganese phosphate hydrate as lithium ion battery anode. *Mater Lett*, 285(15): 129084.1-129084.5. (2021).
16. Jung, Y. H. et al. A multi-element doping design for a high-performance $LiMnPO_4$ cathode via metaheuristic computation. *J. Mater. Chem. A*. **5** (19), 8939–8945 (2017).
17. Zeng, T. et al. $LiMn_{0.8}Fe_{0.2}PO_4$@C cathode prepared via a novel hydrated $MnHPO_4$ intermediate for high performance lithium-ion batteries. *Inorg. Chem. Front.* **10** (4), 1164–1175 (2023).
18. Nag, S. & Roy, S. La-doped $LiMnPO_4$/C cathode material for Lithium-ion battery. *Chem Eng. Sci*, **272**: (2023). 118600.1-118600.6.
19. Chen, J. et al. High performance of $LiMn_{1-x}Fe_xPO_4$/C ($0 \le x \le 0.5$) nanoparticles synthesized by microwave-assisted solvothermal method. *Ionics* **24** (3), 689–696 (2017).
20. Xiang, W. et al. Hierarchical structured $LiMn_{0.5}Fe_{0.5}PO_4$ spheres synthesized by template-engaged reaction as cathodes for high power Li-ion batteries. *Electrochim. Acta*. **178**, 353–360 (2015).
21. Peng, Z. et al. Green and efficient synthesis of micro-nano $LiMn_{0.8}Fe_{0.2}PO_4$/C composite with high-rate performance for Li-ion battery. *Electrochim Acta*, 387: 138456.1-138456.10. (2021).
22. Padhi, A. K., Nanjundaswamy, K. S. & Goodenough, J. B. Phospho-olivines as positive-electrode materials for rechargeable Lithium batteries. *J. Electrochem. Soc.* **144** (4), 1188–1194 (1997).
23. Wang, J. & Sun, X. Olivine $LiFePO_4$: the remaining challenges for future energy storage. *Energ. Environ. Sci.* **8** (4), 1110–1138 (2015).
24. Layadi, T. M. et al. Design of sustainable multi-source power systems using lithium batteries. *J Energy Storage*, 60(3): 106648.1-106648.14. (2023).
25. Huang, Y. et al. Integrated rocksalt–polyanion cathodes with excess lithium and stabilized cycling. *Nat. Energy*. **9** (12), 1497–1505 (2024).
26. Yang, J. et al. Zero Lithium miscibility gap enables High-Rate equimolar $Li(Mn,Fe)PO_4$ solid Solution. *Nano Lett.* **21** (12), 5091–5097 (2021).
27. Oukahou, S. et al. Investigation of $LiMn_{1-x}M_xPO_4$ (M = Ni, Fe) as cathode materials for Li-ion batteries using density functional theory. *Comp Mater. Sci*, **202**: (2022). 111006.1-111006.11.
28. Pleuksachat, S. et al. Dynamic phase transition behavior of a $LiMn_{0.5}Fe_{0.5}PO_4$ olivine cathode material for lithium-ion batteries revealed through in-situ X-ray techniques. *J. Energy Chem.* **71**, 452–459 (2022).
29. Zhu, J. N. et al. Synthesis of $LiMnPO_4$/C with superior performance as Li-ion battery cathodes by a two-stage microwave solvothermal process. *J. Mater. Chem. A*. **3** (26), 13920–13925 (2015).
30. Li, S. N. et al. Synthesis and electrochemical properties of $LiFePO_4$ cathode material by ionic thermal method using eutectic mixture of tetramethyl ammonium chloride-urea. *Rare Met.* **40** (12), 3477–3484 (2021).
31. Sharmila, V. & Parthibavarman, M. Lithium manganese phosphate associated with MWCNT: Enhanced positive electrode for lithium hybrid batteries. *J Alloy Compd*, 858: 157715.1-157715.10. (2021).
32. Zhang, J. N. et al. Trace doping of multiple elements enables stable battery cycling of $LiCoO_2$ at 4.6 V. *Nat. Energy*. **4** (7), 594–603 (2019).
33. Lu, X. et al. Ethylene glycol solvothermal synthesis of $LiMnPO_4$ nanoparticles with high (2 0 0) crystal face exposure for high performance lithium-ion batteries. *Mat Sci. Eng. B*, **299**: (2024). 117032.1-117032.7.
34. Wen, F. et al. Graphene-embedded $LiMn_{0.8}Fe_{0.2}PO_4$ composites with promoted electrochemical performance for lithium ion batteries. *Electrochim. Acta*. **276**, 134–141 (2018).
35. Pan, X. et al. Self-templating Preparation and electrochemical performance of $LiMnPO_4$ Hollow microspheres. *J. Alloy Compd.* **783**, 468–477 (2019).
36. Chi, Z. X. et al. Accurate surface control of core-shell structured $LiMn_{0.5}Fe_{0.5}PO_4$@C for improved battery performance. *J. Mater. Chem. A*. **2** (41), 17359–17365 (2014).
37. Zhang, B. et al. [001]-oriented $LiMn_{0.6}Fe_{0.4}PO_4$/C Nanorod microspheres contributing high-rate performance to olivine-structured cathode for lithium-ion battery. *Mater Today Energy*, **30**: (2022). 101162.1-101162.12.
38. El, K. R. et al. Nickel-substituted $LiMnPO_4$/C olivine cathode material: combustion synthesis, characterization and electrochemical performances. *Ceram. Int.* **45** (14), 17688–17695 (2019).
39. Li, Y. et al. Simple synthesis of a hierarchical $LiMn_{0.8}Fe_{0.2}PO_4$/C cathode by investigation of iron sources for lithium-ion batteries. *RSC Adv.* **12** (40), 26070–26077 (2022).
40. Wang, Y. et al. Rational design of a synthetic strategy, carburizing approach and pore-forming pattern to unlock the cycle reversibility and rate capability of micro-agglomerated $LiMn_{0.8}Fe_{0.2}PO_4$ cathode materials. *J. Mater. Chem. A*. **6** (22), 10395–10403 (2018).
41. Shi, S. et al. Multi-scale computation methods: Their applications in lithium-ion battery research and development. *Chinese Physics B*, **25** (1) 018212.1-018212.24. (2016).

42. Hong, Y. et al. High-yield synthesis of $LiMnPO_4$/C nanoplates as cathode materials for lithium-ion batteries. *Scripta Mater*, **241** (2024). 115878.1-115878.7.
43. Zhu, C. et al. Solvothermal-assisted morphology evolution of nanostructured $LiMnPO_4$ as high-performance lithium-ion batteries cathode. *J. Mater. Sci. Technol.* **34** (9), 1544–1549 (2018).
44. Hong, Y. et al. High-performance $LiMnPO_4$ nanorods synthesized via a facile EG-assisted solvothermal approach. *J. Mater. Chem. A*. **3** (19), 10267–10274 (2015).
45. Liao, L. et al. Facile solvothermal synthesis of ultrathin $LiFe_xMn_{1-x}PO_4$ nanoplates as advanced cathodes with long cycle life and superior rate capability. *J. Mater. Chem. A*. **3** (38), 19368–19375 (2015).
46. Niu, Y. H. et al. Controllable synthesis of aluminium-doped $LiMnPO_4$/C cathode materials with stable electrochemical performance for lithium-ion battery. *Mat Sci. Eng. B*, **299**(1) 117009.1-117009.8. (2024).
47. Wang. L. et al. Improved electrochemical performance and capacity fading mechanism of nano-sized $LiMn_{0.9}Fe_{0.1}PO_4$ cathode modified by polyacene coating[J]. *J. Mater. Chem. A*. **3**(4), 1569–1579 (2015).
48. Li J, et al. Facile synthesis of carbon-$LiMnPO_4$ nanorods with hierarchical architecture as a cathode for high-performance Li-ion batteries[J]. *Electrochim Acta*, **289**, 415–421 (2018).
49. Nwachukwu, I. M. et al. The potentials of $LiMnPO_4$ cathode material for aqueous Li-ion batteries: an investigation into solid state and green chemistry approaches. *Appl Surf. Sci. Adv*, **19**, 100537.1-100537.12 (2024).
50. Manjunatha, H., Venkatesha, T. V. & Suresh, G. S. Electrochemical studies of $LiMnPO_4$ as aqueous rechargeable lithium-ion battery electrode. *J. Solid State Electr.* **16** (5), 1941–1952 (2011).
51. Zhang, L. et al. Confined synthesis of hierarchical structured $LiMnPO_4$/C granules by a facile surfactant-assisted solid-state method for high-performance lithium-ion batteries. *J. Mater. Chem. A*. **2** (3), 711–719 (2014).
52. Vásquez, F. A. & Calderón, J. A. Vanadium doping of $LiMnPO_4$ cathode material: Correlation between changes in the material lattice and the enhancement of the electrochemical performance. *Electrochim Acta*, 325: 134930.1-134930.10. (2019).
53. Muruganantham, R., Sivakumar, M. & Subadevi, R. Polyol technique synthesis of Nb_2O_5 coated on $LiFePO_4$ cathode materials for Li-ion storage. *Ionics* **24** (4), 989–999 (2017).

Author contributions
Conceptualization, methodology, validation, L.J-L; writing-original draft, L Z-B and M J-r; review and editing, L J-L; All authors have read and agreed to the published version of the manuscript.

Funding
This work was supported by the funding program of "Carbon Neutral Engineering Research Center of Guizhou colleges and universities in Coal Industry (Qian Jiao Ji [2023] No. 044)", "Guizhou Provincial Science and Technology Projects (Qiankehejichu-ZK [2022] Yiban531) and "the High-level Talents Scientific Research Startup Foundation of Liupanshui Normal University (Grant No. LPSSYKYJJ202006).

Declarations

Competing interests
The authors declare no competing interests.

Additional information
Correspondence and requests for materials should be addressed to J.L.

Reprints and permissions information is available at www.nature.com/reprints.

Publisher's note Springer Nature remains neutral with regard to jurisdictional claims in published maps and institutional affiliations.